Charge-orbital ordering near the multicritical point in *A*-site ordered perovskites $SmBaMn_2O_6$ and $NdBaMn_2O_6$

D. Akahoshi,[1] Y. Okimoto,[1] M. Kubota,[2] R. Kumai,[1] T. Arima,[2,3] Y. Tomioka,[1] and Y. Tokura[1,2,4]
[1]*Correlated Electron Research Center (CERC), National Institute of Advanced Industrial Science and Technology (AIST), Tsukuba 305-8562, Japan*
[2]*Spin Superstructure Project (SSS), ERATO, Japan Science and Technology Corporation (JST), C/O AIST, Tsukuba 305-8562, Japan*
[3]*Institute of Materials Science, University of Tsukuba, Tsukuba 305-8573, Japan*
[4]*Department of Applied Physics, University of Tokyo, Tokyo 113-8656, Japan*
(Received 28 February 2004; revised manuscript received 17 May 2004; published 26 August 2004)

Electronic and magnetic structures of *A*-site ordered perovskite-type manganites, $LnBaMn_2O_6$ (Ln=Sm and Nd), located close to the multicritical point of the competing phases, have been investigated by measurements of resonant x-ray scattering, optical spectroscopy, and neutron diffraction. In the $SmBaMn_2O_6$ crystal, two resonant peaks, (5/4 5/4 0) and (3/2 1/2 1/2) in the tetragonal $a_p \times a_p \times 2a_p$ setting ($a_p \approx 3.9$ Å), are observed at room temperature and are attributed to the *AABB*-type stacking of *ab* planes with a checkerboard-type charge and stripe-type orbital orders. The change of the stacking manner from *AABB*- to *ABAB*-type around 190K is evidenced by the disappearance of the resonant peak (3/2 1/2 1/2) and a steep increase in Raman scattering intensity of a Jahn-Teller phonon mode below 190 K. The powder neutron diffraction study has shown that $NdBaMn_2O_6$ has an A-type antiferromagnetic state below 275 K. The abrupt expansion of the *ab* plane and shrinkage along the *c* axis upon the antiferromagnetic transition at 275 K suggest that uniform $d_{x^2-y^2}$ orbital ordering occurs.

DOI: 10.1103/PhysRevB.70.064418 PACS number(s): 75.30.Kz, 71.27.+a, 78.20.−e

I. INTRODUCTION

Perovskite-type manganites have been extensively studied due to rich and attractive physical properties caused by the close interplay among spin, charge, orbital, and lattice degrees of freedom.[1,2] Among them, the colossal magnetoresistance (CMR) effect, i.e., a large reduction in resistivity by an application of an external field, is one of the main issues. It is generally recognized that there are two important ingredients in CMR physics. One is the phase competition between the ferromagnetic metallic (FM) and the charge-orbital ordered (CO-OO) states. The CMR effect is observed near the bicritical region where the FM and CO-OO phases compete with each other. Another key is the effect of random potential due to quenched disorder near such a critical region. The quenched disorder arises from the impurity substitution on the *B*-site and/or the mismatch effect of the *A*-site cations. The relaxor ferromagnetic behavior of Cr-doped $Nd_{1/2}Ca_{1/2}MnO_3$ or $Pr_{1/2}Ca_{1/2}MnO_3$ is one of the typical examples of the impurity substitution.[3–6] The doping of Cr^{3+} as the immobile orbital vacancies destroys the CO-OO state and causes a dramatic phase conversion from the CO-OO to FM state. On the other hand, the mismatch effect is defined as the *A*-site cation size variance, $\sigma^2 = \Sigma_i x_i r_i^2 - (\Sigma_i x_i r_i)^2$ Here, x_i and r_i denote the fraction and the ionic radius of the *i*th ion of the perovskite *A*-site.[7,8] The important role of the lattice mismatch in the CMR phenomena has recently been demonstrated by the comparative experiments, using $Pr_{0.55}(Ca_{1-y}Sr_y)_{0.45}MnO_3$ and $Ln_{0.55}Sr_{0.45}MnO_3$ (Ln =rare earth).[9,10] In the case of $Pr_{0.55}(Ca_{1-y}Sr_y)_{0.45}MnO_3$ with a smaller mismatch, the competing FM and CO-OO orders form a bicritical point around $\langle r_A \rangle = 1.33$ Å ($\langle r_A \rangle = \Sigma_i x_i r_i$). In the case of $Ln_{0.55}Sr_{0.45}MnO_3$ with a larger mismatch, by contrast, the long-range orders are strongly suppressed, and the fluctuation of the competing orders is most enhanced near the original bicritical region at $\langle r_A \rangle = 1.33$ Å. Such a large phase fluctuation triggers a huge response to the external fields.

However, all of the above-mentioned manganites intrinsically contain the randomness, more or less, originating in the *A*-site disorder. Therefore, to quantify the dramatic effect of the quenched disorder on the CMR physics, a detailed study on manganites that are free of the quenched disorder is preferable. The *A*-site ordered manganite, $LnBaMn_2O_6$, is a good candidate for this purpose. The crystal structure consists of alternating stacks of *Ln*O and BaO sheets along the *c* axis, with intervening MnO_2 sheets (the inset of Fig. 1). As clearly seen from the structural features, $LnBaMn_2O_6$ does not contain the random Coulomb potential and local lattice distortion arising from the *A*-site (Ln^{3+}/Ba^{2+}) disorder. Figure 1 shows the electronic phase diagram for $LnBaMn_2O_6$.[11,12] $LaBaMn_2O_6$ is a ferromagnetic metal with T_C (Curie temperature) =350 K,[13] whereas the ground state of $YBaMn_2O_6$ is a CO-OO insulator. The CO-OO state is seen for Ln=Y-Sm as well. The charge-orbital ordering transition temperature (T_{CO}) is extremely high, reaching 500 K (Ln=Y),[14] compared with those of the conventional *A*-site solid solution manganites. The high T_{CO} is likely due to the absence of *A*-site disordering, which destabilizes the long-range orders and causes the phase fluctuation. Such a high transition temperature that is due to the *A*-site cation ordering reminds us of the case of the high-T_C superconductor, $LnBa_2Cu_3O_7$, compared with the case of the *A*-site solid solution, e.g., $La_{2-x}Sr_xCuO_4$. Both the T_{CO} and T_C monotonously decrease toward the phase boundary, and the CO-OO and FM orders compete with each other in a bicriti-

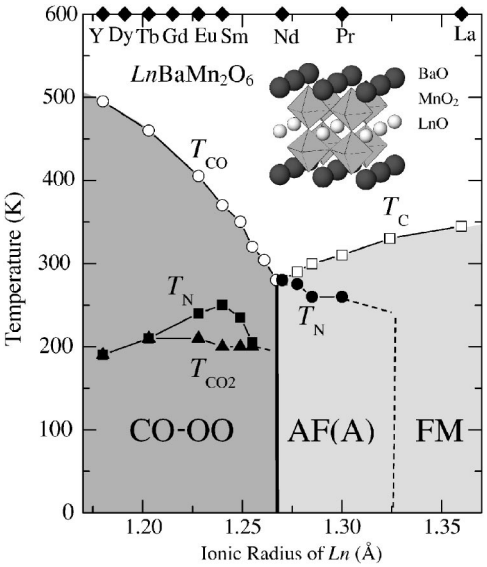

FIG. 1. Electronic phase diagram for the *A*-site ordered perovskite $LnBaMn_2O_6$ (*Ln*=Y and rare earth). The data of the *Ln*/Ba ordered but *Ln*-site mixed compound with *Ln*=(Nd, Sm), (Pr, Nd), and (La, Pr) are included. CO-OO, FM, and AF represent charge-orbital ordered, ferromagnetic metallic, and antiferromagnetic states, respectively. T_{CO}, T_C, and T_N denote the respective transition temperatures. The stacking manner of the CO-OO MnO_2 sheets changes from *AABB*- to *ABAB*-type at T_{CO2}. The inset shows the schematic crystal structure of $LnBaMn_2O_6$.

cal manner around *Ln*=Nd, where $T_{CO} \approx T_C \approx 300$ K. In addition, the A-type antiferromagnetic (AF) phase emerges near the phase boundary (*Ln*=Pr-Nd). The T_C and T_N (Néel temperature) approach each other toward the phase boundary, and finally almost coincide with each other around *Ln*=Nd, forming the multicritical point where the FM, CO-OO, and A-type AF orders meet. The multicritical (bicritical) feature in the clean potential system, such as manganites with small randomness, is theoretically anticipated as well, and the phase diagrams for $LnBaMn_2O_6$ and $Pr_{0.55}(Ca_{1-y}Sr_y)_{0.45}MnO_3$ are qualitatively in good agreement with the theoretical results.[15–17]

The *A*-site cation ordering produces not only the multicritical behavior but also a new combination among the spin, charge, orbital, and lattice degrees of freedom. The powder neutron and electron diffraction measurements revealed that $LnBaMn_2O_6$ has an unprecedented CO-OO phase.[18–21] Several models for the CO-OO structure have been proposed so far, but the issue still remains unsettled. To investigate the detailed CO-OO structure, resonant x-ray, and Raman scattering measurements that can probe, respectively, electronic modulation and local lattice dynamics, will be useful. In this paper, we report the detailed study on $SmBaMn_2O_6$ and $NdBaMn_2O_6$, both locating near that multicritical point (see Fig. 1), by measurements of resonant x-ray scattering, optical spectroscopy, and powder neutron diffraction.

II. EXPERIMENT

A. Sample preparation and characterization

Polycrystalline samples were prepared by a solid-state reaction using Sm_2O_3 (Nd_2O_3), $BaCO_3$, and Mn_3O_4 as the starting materials. Mixed powders composed of the starting materials in prescribed molar ratios were pelletized and treated in Ar atmosphere at 1693 (1743) K with several intermediate grindings and then annealed in O_2 at 973 K.

Single-crystalline $SmBaMn_2O_6$ was prepared in the following way. The mixed powders were calcined at 1273 K in air, pressed into a rod, and sintered at 1693 K under Ar atmosphere. At first, the *A*-site alloyed crystal of $Sm_{1/2}Ba_{1/2}MnO_3$ was grown at a rate of 4–10 mm/h in air by a floating-zone method. The melt-quenched sample was treated in Ar atmosphere at 1693 K for 10 h to encourage the *A*-site ordering, and then annealed in O_2 at 973 K for 2 h. The sample characterization was performed by powder x-ray diffraction. Rietveld analyses of the powder x-ray diffraction data of $SmBaMn_2O_6$ with Rietan2000 and the powder neutron diffraction data of $NdBaMn_2O_6$ with Rietan2001T indicated the perfect ordering of the *Ln* and Ba atoms.[22,23] The magnetic and transport properties of the polycrystalline samples were measured in the ranges of $5\ \mathrm{K} \leqslant T \leqslant 400$ K and $0\ \mathrm{T} \leqslant H \leqslant 7$ T with the use of a Quantum Design SQUID magnetometer (MPMS) and physical property measuring system (PPMS), respectively.

B. Resonant x-ray and neutron diffraction

Resonant x-ray scattering measurements were performed at Beam Line-1A at the Photon Factory, KEK, Tsukuba, Japan. We used an x ray with a photon energy near the Mn *K*-absorption edge. The incident beam was monochromated by a double Si(1 1 1) crystal. The energy resolution was 2 eV. The $SmBaMn_2O_6$ crystal was mounted on the four-axis diffractometer. The sample temperature ($140\ \mathrm{K} \leqslant T \leqslant 400$ K) was controlled by a cold nitrogen blower within an accuracy of 2 K. We mainly investigated the superlattice peaks, (5/4 5/4 0), (5/4 1/4 0), and (3/2 1/2 1/2). In this paper, the observed peaks are indexed in the pseudotetragonal setting, $a_p \times a_p \times 2a_p$, where a_p denotes the cell parameter in a simple cubic setting. The contribution of fluorescence was subtracted from the energy dependence of (5/4 5/4 0), (5/4 1/4 0), and (3/2 1/2 1/2) peaks by using the background data taken at (1.26 1.26 0), (1.26 0.26 0), and (1.51 0.51 0.51), respectively.

The powder neutron diffraction study on $NdBaMn_2O_6$ was performed by a time-of-flight (TOF) diffractometer Vega, KEK, Japan. The temperature was controlled by a closed-cycle 4-K refrigerator within an accuracy of 0.2 K. Structural parameters were obtained by Rietveld analysis using Rietan-2001T.[23]

C. Optical spectroscopy

All of the optical spectra were measured on the (0 0 1) cleaved surface. To measure the temperature dependence ($5\ \mathrm{K} \leqslant T \leqslant 293$ K), we used a conduction-type cryostat. The sample was fixed with vacuum grease within the cryostat to keep the appropriate thermal conduction. $\mathbf{E} \| ab$ reflectivity spectra were measured using a Fourier-transform interferometer (0.05–0.8 eV) and a grating monochromator (0.6–5 eV). Optical conductivity spectra $[\sigma(\omega)]$ were calculated in terms

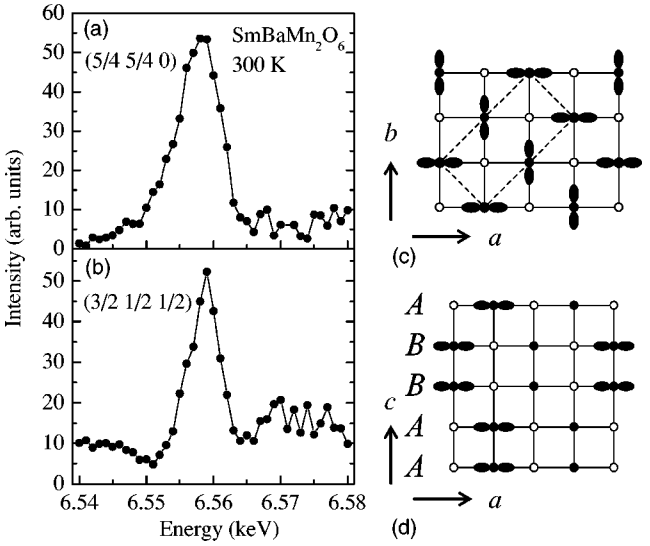

FIG. 2. X-ray photon energy dependence of intensity of the CO-OO superlattice reflections (a) (5/4 5/4 0) and (b) (3/2 1/2 1/2) for $SmBaMn_2O_6$ near the Mn *K*-absorption edge at room temperature, and (c), (d) the corresponding schematic structures of the CO-OO pattern in the *ab* and *ac* plane, respectively. Open circles represent Mn^{4+}, and solid circles and lobes represent $d_{3x^2-r^2}$ and $d_{3y^2-r^2}$ orbitals of the e_g-electron of Mn^{3+}, respectively.

of the Kramers-Kronig analysis of the reflectivity data. Raman spectra were obtained using a He-Ne laser ($\lambda = 632.8$ nm). The polarization of the incident and scattering light is parallel to the [1 1 0] direction in the pseudotetragonal index. Scattered light in the backward configuration was collected through a notch filter and dispersed by a single monochromator equipped with a cooled charge-coupled device detector.

III. RESULT AND DISCUSSION

A. $SmBaMn_2O_6$

1. Resonant x-ray scattering

Figures 2(a) and 2(b) show the x-ray photon energy dependence of superlattice peaks (5/4 5/4 0) and (3/2 1/2 1/2) of $SmBaMn_2O_6$ at room temperature. The four-times periodicity ($2\sqrt{2}a_p$) along [1 1 0] direction has also been observed in the electron diffraction measurements.[19,21] The energy dependence of the both superlattice peaks exhibits resonance with the Mn *K*-absorption edge as seen in Fig. 2, which is attributed to the periodic modulation of the electronic structure occurring in the Mn square lattices. We also observed an azimuthal angle dependence of the two peaks, which should reflect the anisotropic density distribution of electrons. The resonant peak of (5/4 5/4 0), that is, the four-times periodicity of the electronic modulation along the [1 1 0] direction, is strong evidence for the checkerboard-type charge ordering of Mn^{3+}/Mn^{4+} with diagonal $d_{3x^2-r^2}/d_{3y^2-r^2}$ orbital ordering as shown in Fig. 2(c).[24] The CO-OO pattern in the *ab* planes of $SmBaMn_2O_6$ is thus the same as that of the *A*-site disordered manganites in the vicinity of half-doping, such as $La_{1/2}Ca_{1/2}MnO_3$ and $Pr_{1/2}Ca_{1/2}MnO_3$.[25–28] What is specific to $SmBaMn_2O_6$ is that the resonant peak of (3/2 1/2 1/2) is observed. [Note that the superlattice peak (3/2 1/2 1/2) would be translated into (3/2 1/2 1/4) in the simple cubic setting.] This means that the *A*-site cation ordering or the stacking of the CO-OO MnO_2 sheets show the four-times periodicity ($4a_p$) along the *c* axis. If the four-times periodicity were attributed to the *A*-site cation ordering, (0 0 1/2) peak [(0 0 1/4) in the pseudocubic setting] could be observed by x-ray and electron diffraction. However, such a peak was not discerned. Furthermore, the high-resolution transmission electron microscopy (HRTEM) image directly shows the alternate stack of *Ln*O and BaO sheets at room temperature.[11] From these reasons, it is concluded that the four-times periodicity results from the periodic modulation of the stack of the CO-OO MnO_2 sheets, not from the *A*-site cation ordering. The stacking manner of the CO-OO planes is thus different from that of $La_{1/2}Ca_{1/2}MnO_3$ and $Pr_{1/2}Ca_{1/2}MnO_3$ in which the CO-OO MnO_2 sheets stack without a phase shift along the *c* axis. Under these circumstances, the most plausible model for the stacking at room temperature is the *AABB*-type model [Fig. 2(d)]. In this model, each pair of *ab* planes (*AA* or *BB*) stacks with a phase shift of $\pm a$ along the *c* axis.

To be more quantitative, we show in Fig. 3 the temperature dependence of magnetization (M), resistivity (ρ), derivative of resistivity ($d \ln \rho / dT$) and intensities of the resonant x-ray peaks for $SmBaMn_2O_6$. All of the superlattice peaks disappear above 380 K, where the M and ρ show steep changes. Those changes at 380 K are ascribed to the onset of the charge-orbital ordering.[11,19] The broad peak in the M-T curve around 250 K corresponds to the AF transition.[18] The intensity of the superlattice peak (5/4 5/4 0) is almost constant between 140 and 300 K, proving that the CO-OO pattern in the *ab* plane does not change in this temperature range. In contrast, the superlattice peak (3/2 1/2 1/2) suddenly disappears below 190 K, and the ρ or $d \ln \rho / dT$ shows an anomaly at this temperature. The disappearance of the (3/2 1/2 1/2) peak is attributed to the change of the stacking pattern of the CO-OO MnO_2 sheets. Hereafter, we refer to the switching temperature as "T_{CO2}." To understand the origin of such a stacking change, it is worth noting here that T_{CO2} is lower than T_N in the present case while the two temperatures coincide in $TbBaMn_2O_6$.[18] This implies that the onset or the evolution of spin ordering favors the low-temperature stacking pattern of charge-orbital ordering.

There are two possible models for the stacking pattern below T_{CO2}. One is the *AAAA*-type stacking in which the CO-OO MnO_2 planes stack without a phase shift, just like in the conventional half-doped manganite case. The other is the *ABAB*-type stacking in which the staggered charge ordering of Mn^{3+}/Mn^{4+} is of rock-salt type and hence the two-times periodicity of the MnO_2 sheet stacking coincides with that of the *A*-site cation ordering [Fig. 3(a)]. The resonant x-ray peaks cannot provide decisive evidence for which type of stacking pattern is realized below T_{CO2}, because the superlattice peak (3/2 1/2 1/2) vanishes in both models. In $TbBaMn_2O_6$ where the switching of the stacking occurs con-

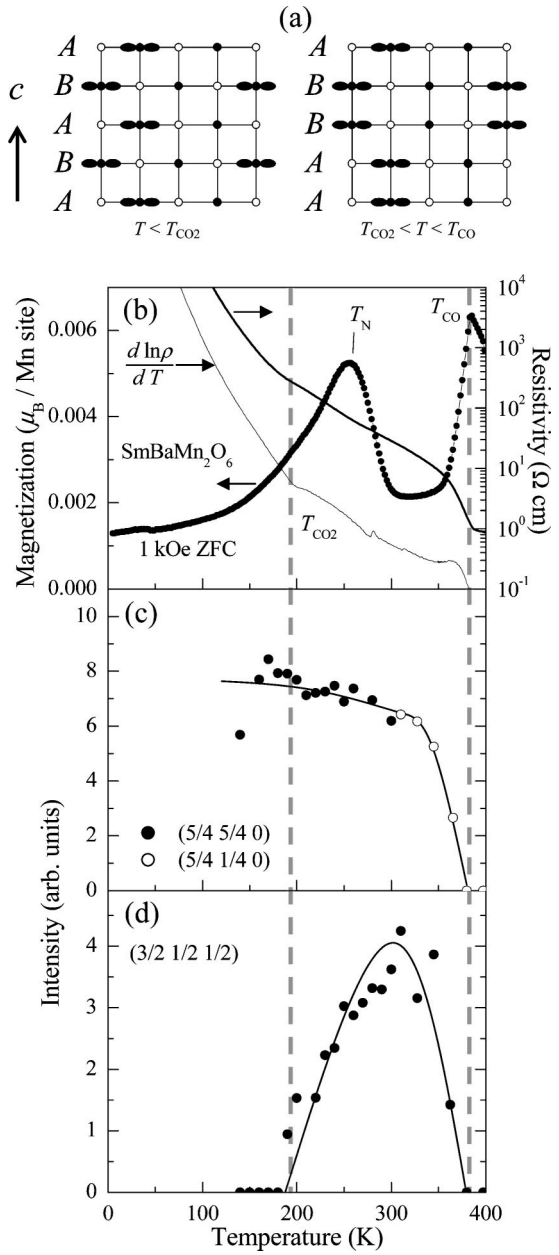

FIG. 3. (a) Schematic CO-OO structures in the *ac* plane. Temperature dependence of (b) magnetization (M), resistivity (ρ), derivative of the resistivity ($d \ln \rho / dT$), and intensity (I) of the resonant x-ray superlattice peaks (c) (5/4 5/4 0), (5/4 1/4 0), and (d) (3/2 1/2 1/2) for $SmBaMn_2O_6$. Solid lines in (c) and (d) are a guide to the eye.

comitantly with the AF spin ordering, Arima *et al.* proposed that the *ABAB*-type stack is relevant below T_N by taking the AF spin configuration into account.[18] It is reasonable to consider that the stacking pattern of $SmBaMn_2O_6$ is the same as that of $TbBaMn_2O_6$. Other evidence supporting this model is shown in terms of optical spectroscopy in the following section.

2. Spectra of optical conductivity and Raman scattering

Figure 4(a) shows spectra of $\mathbf{E} \| ab$ optical conductivity $[\sigma(\omega)]$ in $SmBaMn_2O_6$ at 293 and 5 K. (The spiky structures around 0.07 eV are due to optical phonon modes.) At room temperature, a broad peak is observed at $\approx$1.1 eV. With the decrease of temperature, the peak shows a blue shift and $\sigma(\omega)$ shows a clear gaplike structure. The value of the optical gap is estimated to be $\approx$0.6 eV by the extrapolation procedure shown with a dashed line in Fig. 4(a). It is worth noting that such temperature dependence and spectral shapes are quite similar to those observed for $Pr_{0.6}Ca_{0.4}MnO_3$[29] and $La_{0.5}Sr_{1.5}MnO_4$[30,31] with conventional CE-type spin, checkerboard-type charge, and stripe-type orbital ordering. According to previous works, the broad peak around 1.1 eV is assigned to the transfer of the $d_{3x^2-r^2}$ (or $d_{3y^2-r^2}$) electron to the neighboring Mn^{4+} site along the direction of the orbital lobe [see Fig. 2(c)]. This indicates that the *A*-site ordering or the difference in the stacking pattern of the CO-OO *ab* plane sheets scarcely affect the *ab* plane electronic spectrum.

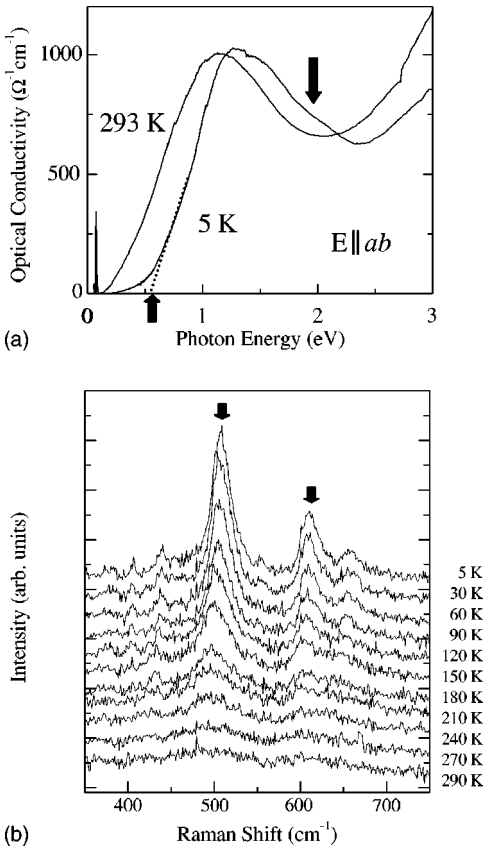

FIG. 4. (a) $\mathbf{E} \| ab$ optical conductivity $[\sigma(\omega)]$ at 293 K and 5 K in $SmBaMn_2O_6$. The dashed line shows the extrapolation procedure for the estimate of the gap transition energy (indicated by an upward arrow). (b) Temperature dependence of Raman spectra on the *ab* plane of $SmBaMn_2O_6$. The polarizations of the incident and scattering light are both parallel to the [110] direction in the pseudotetragonal setting. The exciting light source is a He-Ne laser, whose photon energy position is indicated by a downward arrow in the optical conductivity spectra (a).

Keeping this in mind, we show in Fig. 4(b) the temperature dependence of the Raman spectra in $SmBaMn_2O_6$. At the ground state (5 K), the Raman spectral shape also resembles that of a layered manganite, $La_{0.5}Sr_{1.5}MnO_4$,[32] where two major peaks are observed around 500 and

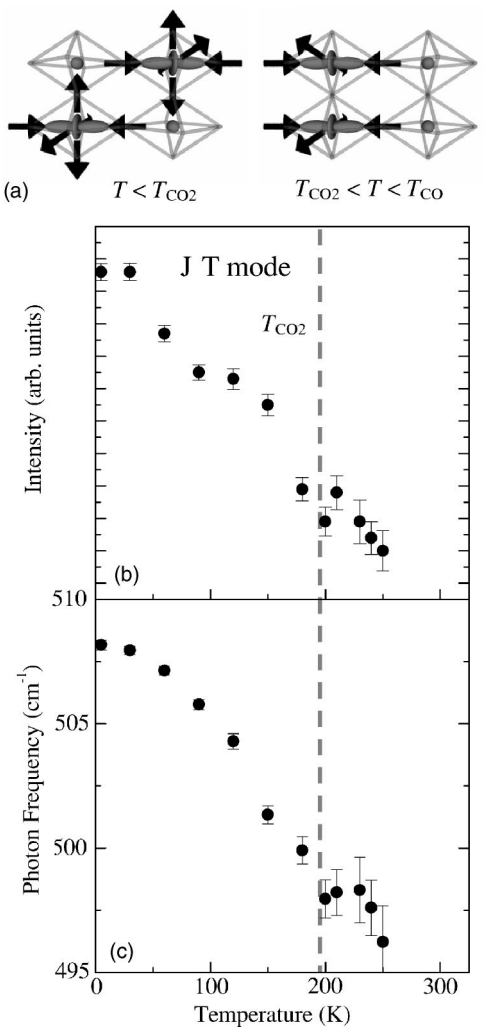

FIG. 5. (a) Patterns of normal mode vibrations of the JT mode above and below T_{CO2}. Temperature profiles of (b) Raman scattering intensity (S) of the JT phonon mode and (c) its frequency (ω). A vertical dashed line indicates the switching temperature T_{CO2} of the CO-OO *ab* plane stacking along the *c* axis.

620 cm^{-1}. According to the previous work,[32] those Raman peaks are assigned to the Jahn-Teller (JT) and breathing modes, respectively. However, the temperature dependence differs greatly from the case of the layered manganite. Those two modes are rapidly suppressed with increasing temperature toward T_{CO2} and bear little intensity in the temperature range of $T_{CO2} < T < T_{CO}$. To be more quantitative, we plot in Fig. 5 the temperature dependence of spectral intensity (S) and frequency (ω) in the JT mode, which were obtained in terms of Lorentzian fitting procedures. Below T_{CO2}, S and ω are remarkably increased. In the prototypical CE-type state of $La_{0.5}Sr_{1.5}MnO_4$, the temperature dependence of S reproduces the change of order parameter of the orbital ordering.[32] As mentioned in the previous section, by contrast, the intensity of the superlattice reflection (5/4 5/4 0), which represents the order parameter, shows little temperature variation below 293 K in $SmBaMn_2O_6$ [see Fig. 3(c)]. This indicates that the temperature variation of S in $SmBaMn_2O_6$ cannot be ascribed to the evolution of the *ab* plane CO-OO state. One might consider a resonant effect as a possible origin of the temperature variation in the Raman spectra. As shown in a downward arrow in Fig. 4(a), however, $\sigma(\omega)$ is scarcely changed with temperature at 1.96 eV ($\lambda = 632.8$ nm). This may exclude the resonant effect as the major origin of the large variation of S between the low-temperature *ABAB* and high-temperature *AABB* CO-OO phases.

A plausible scenario for the unconventional temperature dependence of S is a change in the pattern of the normal mode, which is driven by the structural phase transition. In the case of $SmBaMn_2O_6$, we can consider two different JT modes below and above T_{CO2}, as depicted in Fig. 5(a). In the *AABB*-type stack above T_{CO2}, apical oxygen atoms connecting $Mn^{3+}O_6$ octahedra along the *c* axis do not move in the normal mode, which is similar to the case of a bilayered manganite.[32] By contrast, in the *ABAB*-type stack of the CO-OO *ab* plane sheets below T_{CO2}, where respective $Mn^{3+}O_6$ octahedra are not directly connected to each other, all six oxygens surrounding Mn^{3+} can participate in the normal mode vibration. Both modes are Raman active, but S should be different. Phenomenologically speaking, S is proportional to $|(\partial\varepsilon/\partial Q)Q|^2$, where ε and Q are the dielectric function and amplitude of a normal mode vibration, respectively. As inferred from the patterns of the two normal modes [Fig. 5(a)], the coupling strength with the e_g orbital (i.e., $|\partial\varepsilon/\partial Q|$) appears to be larger in the *ABAB* stack below than the *AABB* stack above T_{CO2}. This qualitatively explains the variation of S with temperature. If *AAAA*-type stacking were realized below T_{CO2}, S would be even smaller than that of the *AABB*-type stacking. Therefore, the observed Raman result supports the present model of the structural phase transition, namely, between the *AABB*- and *ABAB*-type stack of CO-OO sheets, as proposed by the resonant x-ray diffraction study [Fig. 3(a)].

B. $NdBaMn_2O_6$

Figure 6(a) shows the temperature dependence of M, ρ, and M^{-1} for $NdBaMn_2O_6$. The abrupt increase in M around 300 K is due to the appearance of the FM state or the growth of the strong ferromagnetic correlation. Then, M and ρ simultaneously show sudden changes around $T_N \approx 275$ K, implying that some magnetic transition occurs at this temperature. To investigate the magnetic structure, we performed a powder neutron diffraction study on $NdBaMn_2O_6$. Figure 7(b) shows the neutron diffraction profiles for $NdBaMn_2O_6$ at various temperatures. The (0 0 1) peak at 292 K is attributed to the Nd/Ba cation ordering. We see that the intensities of the several peaks, such as (0 0 l) and (1 0 l) with l=odd integer, steeply increase below T_N. The temperature dependence of the (1 0 1) peak intensity is plotted in Fig. 6(b). The abrupt increase in the intensity is due to the appearance of the magnetic Bragg peak, which is superimposed on the nuclear Bragg peak. The neutron diffraction pattern below T_N can be fitted in terms of the layered A-type AF structure in which the *ab* plane has a ferromagnetic spin ordering and the ferromagnetic planes are stacked antiferromagnetically along the *c* axis, as shown in Fig. 7(a).

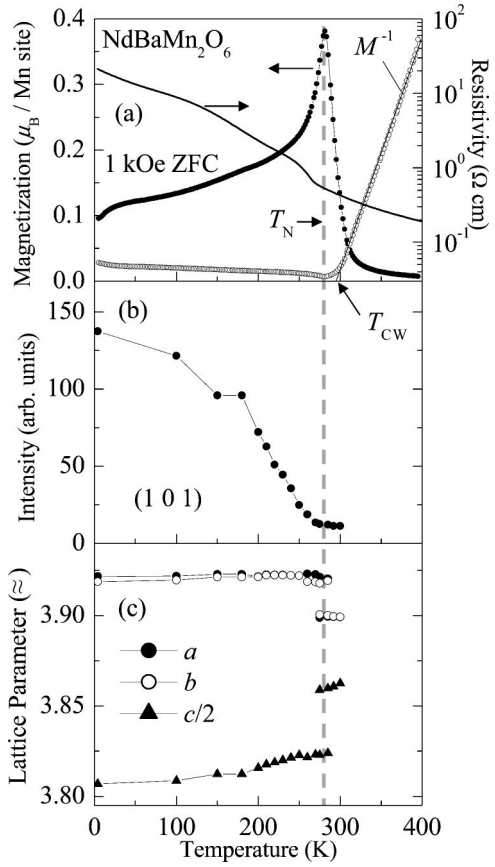

FIG. 6. Temperature dependence of (a) magnetization (M), resistivity (ρ), and inverse magnetization (M^{-1}), (b) intensities of the (1 0 1) Bragg peak, indicating the A-type antiferromagnetic (AF) order, of powder neutron diffraction, and (c) lattice parameters for $NdBaMn_2O_6$. T_N (as shown by a vertical dashed line) and T_{CW} in (a) stand for Néel temperature and ferromagnetic Curie-Weiss temperature, respectively.

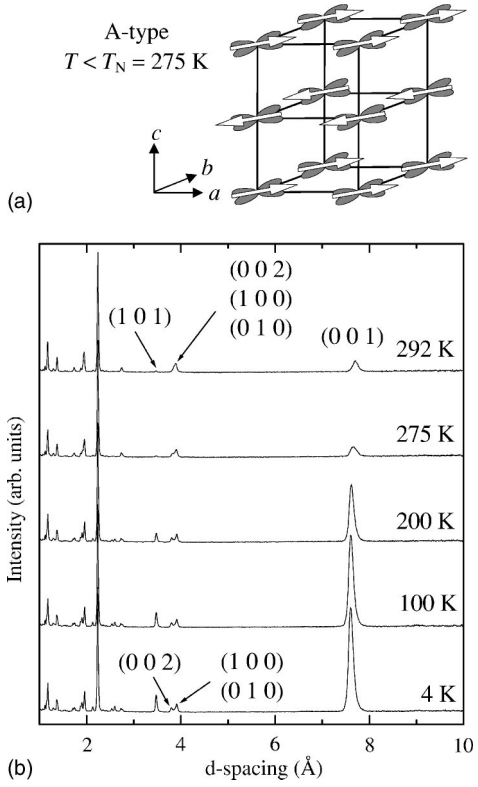

FIG. 7. (a) Schematic structure of the A-type AF structure with uniform $d_{x^2-y^2}$ orbital ordering. Arrows indicate the spin moments on Mn sites. (b) Time-of-flight powder neutron diffraction patterns of $NdBaMn_2O_6$ at various temperatures.

The A-type AF order is often observed in heavily doped-manganites such as $Nd_{0.45}Sr_{0.55}MnO_3$ and $Pr_{1/2}Sr_{1/2}MnO_3$,[33–35] as well as undoped/lightly doped manganites such as $LaMnO_3/La_{1-x}Sr_xMnO_3$ ($x \leqslant 0.05$).[36–38] The A-type AF phase is always accompanied by some orbital ordering. $LaMnO_3$ has an alternate ordering of $d_{3x^2-r^2}/d_{3y^2-r^2}$ orbitals in the *ab* plane and is a Mott insulator. On the other hand, the heavily doped manganites (e.g., $Nd_{0.45}Sr_{0.55}MnO_3$) have a uniform $d_{x^2-y^2}$ orbital order in the *ab* plane [Fig. 7(a)] and show the two-dimensional metallic behavior in the plane.[34] Taking account of the proximity of $NdBaMn_2O_6$ to the metallic ferromagnetism, as well as its high ($x=0.5$) hole doping level, it is natural to consider that the $d_{x^2-y^2}$ orbital ordering is realized in the A-type AF state of the present compound. Figure 6(c) shows the temperature dependence of the lattice parameters for $NdBaMn_2O_6$. The lattice parameters show an abrupt jump at $T_N=275$ K, below which the *ab* plane expands and the *c* axis shrinks. The observation is consistent with the collective JT distortion accompanied by the $d_{x^2-y^2}$ orbital ordering.

Then, we discuss the abrupt change in the M around 300 K. In the magnetic neutron scattering, some of magnetic Bragg peaks, (0 0 2) [(0 0 1) in the simple cubic setting], (1 0 0), and (0 1 0), should emerge in a ferromagnetic state, but vanish in an A-type AF state. Therefore, if long-range ferromagnetic order were realized just above T_N, these peak intensities would drastically change across T_N. However, as clearly seen from Fig. 7(b), the intensities of the (0 0 2), (1 0 0), and (0 1 0) peaks above T_N are almost the same as those below T_N. We can see no anomaly in the ρ-T curve around 300 K [Fig. 6(a)] characteristic of the FM transition. The temperature dependence of the M^{-1} suggests a ferromagnetic correlation, and a ferromagnetic Curie-Weiss temperature (T_{CW}) estimated from the $M^{-1}-T$ curve [a thin straight line in Fig. 6(a)] almost coincides with $T_N=275$ K. From these results, we can conclude that the abrupt increase in M is due not to the long-range ferromagnetic order, but to the strong ferromagnetic correlation. With an increase in the ionic radii of Ln^{3+}, the T_C rises to be detached from T_N. The A-type AF phase disappears between Ln=Pr and La, and the FM phase replaces the A-type AF phase as the ground state. As shown in the phase diagram in Fig. 1, $NdBaMn_2O_6$ is very close to the multicritical point where the three competing orders, i.e., FM, CO-OO, and A-type AF orders, meet.

IV. CONCLUSION

We have investigated the electronic and magnetic structures of $LnBaMn_2O_6$ (Ln=Sm and Nd) by resonant x-ray scattering, optical spectroscopy, and neutron diffraction. The CO-OO structure is unprecedented, reflecting the structural

characteristics. The CO-OO pattern in the *ab* plane is the so-called checkerboard-type associated with the diagonal $d_{3x^2-r^2}/d_{3y^2-r^2}$ orbital ordering, which is often observed in the *A*-site disordered manganites as well in the vicinity of half-doping. However, the stacking pattern of the CO-OO MnO_2 sheets is distinct from the conventional one. In the temperature range of $T_{CO2}=190\ \mathrm{K} \leqslant T \leqslant T_{CO}=380\ \mathrm{K}$ the stacking manner of the *ab* planes is of *AABB*-type. As the temperature is further decreased below T_{CO2}, the stacking pattern turns into the *ABAB*-type. On the other hand, the ground state of $NdBaMn_2O_6$ is the A-type AF state associated with the $d_{x^2-y^2}$ orbital ordering, located in the immediate vicinity of the multicritical region where the FM, CO-OO, and A-type AF orders compete with each other.

ACKNOWLEDGMENTS

We would like to thank M. Uchida, H. Takagi, H. Okamoto, N. Nagaosa, K. Oikawa, and T. Kamiyama for valuable discussions. This work was partly supported by New Energy and Industrial Technology Development Organization (NEDO) and by a Grant-In-Aid for Scientific Research from the MEXT of Japan.

[1] Y. Tokura and N. Nagaosa, Science **288**, 462 (2000).
[2] E. Dagotto, T. Hotta, and A. Moreo, Phys. Rep. **344**, 1 (2001).
[3] B. Raveau, A. Maignan, and C. Martin, J. Solid State Chem. **130**, 162 (1997).
[4] A. Barnebe, A. Maignan, M. Hervieu, F. Damay, C. Martin, and B. Raveau, Appl. Phys. Lett. **71**, 3907 (1997).
[5] T. Kimura, Y. Tomioka, R. Kumai, Y. Okimoto, and Y. Tokura, Phys. Rev. Lett. **83**, 3940 (1999).
[6] T. Kimura, R. Kumai, Y. Okimoto, Y. Tomioka, and Y. Tokura, Phys. Rev. B **62**, 15 021 (2000).
[7] J. P. Attfield, Chem. Mater. **10**, 3239 (1998).
[8] L. M. Rodriguez-Martinez and J. P. Attfield, Phys. Rev. B **63**, 024424 (2000).
[9] Y. Tomioka and Y. Tokura, Phys. Rev. B **66**, 104416 (2002).
[10] Y. Tomioka, Y. Okimoto, J. H. Jung, R. Kumai, and Y. Tokura, Phys. Rev. B **68**, 094417 (2003).
[11] D. Akahoshi, M. Uchida, Y. Tomioka, T. Arima, Y. Matsui, and Y. Tokura, Phys. Rev. Lett. **90**, 177203 (2003).
[12] T. Nakajima, H. Kageyama, H. Yoshizawa, and Y. Ueda, J. Phys. Soc. Jpn. **71**, 2843 (2002).
[13] F. Millange, V. Caignaert, B. Domenges, B. Raveau, and E. Suard, Chem. Mater. **10**, 1974 (1998).
[14] T. Nakajima, H. Kageyama, and Y. Ueda, J. Phys. Chem. Solids **63**, 913 (2002).
[15] J. Burgy, M. Mayr, V. Martin-Mayor, A. Moreo, and E. Dagotto, Phys. Rev. Lett. **87**, 277202 (2001).
[16] Y. Motome, N. Furukawa, and N. Nagaosa, Phys. Rev. Lett. **91**, 167204 (2003).
[17] H. Aliaga, D. Magnoux, A. Moreo, D. Poilblanc, S. Yunoki, and E. Dagotto, Phys. Rev. B **68**, 104405 (2003).
[18] T. Arima, D. Akahoshi, K. Oikawa, T. Kamiyama, M. Uchida, Y. Matsui, and Y. Tokura, Phys. Rev. B **66**, 140408(R) (2002).
[19] M. Uchida, D. Akahoshi, R. Kumai, Y. Tomioka, T. Arima, Y. Tokura, and Y. Matsui, J. Phys. Soc. Jpn. **71**, 2605 (2002).
[20] A. J. Williams and J. P. Attfield, Phys. Rev. B **66**, 220405(R) (2002).
[21] H. Kageyama, T. Nakajima, M. Ichihara, Y. Ueda, H. Yoshizawa, and K. Ohoyama, J. Phys. Soc. Jpn. **72**, 241 (2003).
[22] F. Izumi and T. Ikeda, Mater. Sci. Forum **321-324**, 198 (2000).
[23] T. Ohta, F. Izumi, K. Oikawa, and T. Kamiyama, Physica B **234-236**, 1093 (1997).
[24] Y. Murakami, H. Kawada, H. Kawata, M. Tanaka, T. Arima, Y. Moritomo, and Y. Tokura, Phys. Rev. Lett. **80**, 1932 (1998).
[25] E. O. Wollan and W. C. Koehler, Phys. Rev. **100**, 545 (1955).
[26] P. G. Radaelli, D. E. Cox, M. Marezio, and S-W. Cheong, Phys. Rev. B **55**, 3015 (1997).
[27] Z. Jirak, S. Krupicka, Z. Simsa, M. Dlouha, and S. Vratislav, J. Magn. Magn. Mater. **53**, 153 (1985).
[28] J. P. Hill, C. S. Nelson, M. v. Zimmermann, Y. J. Kim, D. Gibbs, D. Casa, B. Keimer, Y. Murakami, C. Venkataraman, T. Gog, Y. Tomioka, Y. Tokura, V. Kiryukhin, T. Y. Koo, and S. W. Cheong, Appl. Phys. A: Mater. Sci. Process. **73**, 723 (2001).
[29] Y. Okimoto, Y. Tomioka, Y. Onose, Y. Otsuka, and Y. Tokura, Phys. Rev. B **57**, R9377 (1998); **59**, 7401 (1999).
[30] T. Ishikawa, K. Ookura, and Y. Tokura, Phys. Rev. B **59**, 8367 (1999).
[31] J. H. Jung, J. S. Ahn, J. Yu, T. W. Noh, J. Lee, Y. Moritomo, I. Solovyev, and K. Terakura, Phys. Rev. B **61**, 6902 (2000).
[32] K. Yamamoto, T. Kimura, T. Ishikawa, T. Katsufuji, and Y. Tokura, Phys. Rev. B **61**, 14 706 (1998).
[33] H. Kawano, R. Kajimoto, H. Yoshizawa, Y. Tomioka, H. Kuwahara, and Y. Tokura, Phys. Rev. Lett. **78**, 4253 (1997).
[34] H. Kuwahara, T. Okuda, Y. Tomioka, A. Asamitsu, and Y. Tokura, Phys. Rev. Lett. **82**, 4316 (1999).
[35] R. Kajimoto, H. Yoshizawa, H. Kawano, H. Kuwahara, Y. Tokura, K. Ohoyama, and M. Ohashi, Phys. Rev. B **60**, 9506 (1999).
[36] J. B. Goodenough, Phys. Rev. **100**, 564 (1955).
[37] A. Urushibara, Y. Moritomo, T. Arima, A. Asamitsu, G. Kido, and Y. Tokura, Phys. Rev. B **51**, 14 103 (1995).
[38] Y. Murakami, J. P. Hill, D. Gibbs, M. Blume, I. Koyama, M. Tanaka, H. Kawata, T. Arima, Y. Tokura, K. Hirota, and Y. Endoh, Phys. Rev. Lett. **81**, 582 (1998).